ACTIVE VIBRATION CONTROL FOR A FREE PISTON STIRLING ENGINE GENERATOR USING A VOICE COIL ACTUATOR

ALI HASSAN, ANGEL TORRES-PEREZ
STEFAN KACZMARCZYK, PHIL PICTON
The University of Northampton
Northampton, United Kingdom

e-mail: Ali.hassan@northampton.ac.uk

This work presents the study of active vibration control for a FPSE/LA engine to ensure a reliable engine operation within a broader range of operation frequencies [50 ± 3 Hz] complying with new regulations. An ATMD is discussed as a potential solution for increasing the operational envelope from original frequency requirements of [50 ± 0.5 Hz] to the new range while maintaining vibration amplitudes below 20 μm. A suitable vibration model of the engine setup is discussed and experimentally validated. The active vibration control for the vibration model is achieved by integrating the model of a current controlled Voice coil Motor (VCM). Zero-placement with relative acceleration/position and optimal linear quadratic control with a state observer were studied and compared in the time and frequency domains. The analysis shows that the active control accomplishes damping of vibration even at higher frequencies that coincide with the resonance of the entire system. A set of specifications were obtained based on actuator parameters such as power consumption, actuator strokes and force. The effect of time delays on the stability with each control strategy was investigated based on the proposed vibration model. Delays were found to affect stability depending on both the control methodology and excitation frequency.

KEYWORDS
β-type stirling engine, active vibration damping, linear quadratic control, feedback-feedforward with zero-placement, voice coil actuator, electrical current control, effect of time delays

1. INTRODUCTION

Free Piston Stirling Engine Generators are synchronous machines fitted with a linear alternator (FPSE/LA). Commercially available FPSE/LAs for Micro Combined Heat and Power (MCHP) systems have a single phase linear alternator [Harrison 2004]. Stirling engines are power machines that operate over a closed, regenerative thermodynamic cycle, with cyclic compression and expansion of the working fluid at different temperature levels [Walker 1980]. A variety of heat sources can be utilized including solar energy, waste heat, and fossil fuels. From an operational point of view, these machines are always subjected to vibrations due to Lorentz law. The reciprocating motion of the permanent magnets attached to the power piston exerts a force on the alternator coil causing vibration. This type of grid connected machines is designed and tuned to operate within a frequency range of 50 Hz ± 0.5 Hz in Europe. In general, the damping of vibration in equipment is usually accomplished by employing elastic and viscous materials [Rao 1990, Mead 1999]. A tuned mass damper (TMD) is currently employed to attenuate the vibration of the engine case at this frequency. Recently, the European Network of Transmission System Operators for Electricity (ENTSO) has brought new regulations for grid connection and disconnection of low power generators which introduced wider grid operation frequencies. While passive devices such as TMDs provide a simple and a reliable way to tackle many vibration problems, there is distinct performance limitations associated with the use of only passive devices. In its current form, the engine cannot comply with the new regulations. Active vibration control techniques can achieve a far better performance than passive ones by employing adjustable actuators such as hydraulic pistons, piezoelectric device, electromagnetic actuator, etc. that provide an external aiding force. Active damping of vibration has been studied extensively and a surplus of work has been published in this area. [Chang 1995, Yan 1999, Nagashima 2001, Li 2003] studied active TMD systems using classical feedback control methods including displacement, speed, and acceleration feedback. For active vibration control with high positioning accuracy, piezoelectric actuators are often used [Kwak 2007]. In recent years, there has been a growing interest in using electromagnetic actuators instead of piezoelectric actuators. [Park 2008] developed a four-mount active vibration isolation system using voice coil actuators. [Liu 2013] used a voice coil actuator with velocity feedback control for highly sensitive instruments by producing a sky-hook damper at low frequencies (2–6 Hz). Their proposed method reduced the vibration at resonance without causing larger vibration amplitudes at higher frequencies. In terms of Stirling-type applications, Ross [Ross Jr 2003] provided an overview of the vibration characteristics of typical linear-drive space cryo-coolers outlining the history of development and typical performance of the various active and passive vibration suppression systems being used. Recently, Johnson [Johnson 2012] worked on developing embedded active vibration cancellation of a Piston-Driven cryo-cooler or nuclear spectroscopy applications. This study provides a continuation of the work done by [Hassan 2014]. Specifically, a voice coil actuator is integrated into the proposed model of the Stirling engine. In this work, further studies with two different control strategies have been carried out. The analysis showed that from theoretical point of view, the control strategies have accomplished the damping of vibration even at resonant frequencies of the system. The effect of time delays on each control strategy has also been investigated. It was found that delays could affect the stability depending on the control methodology followed and on the frequency of excitation.

2. BACKGROUND THEORY: PASSIVE AND ACTIVE TMD

The working principle of the passive TMD is based on coupling an auxiliary mass to a structure whose vibration needs to be minimized. For the TMD to function properly, synchronization between the natural frequency of the added mass and the excitation frequency of the original structure needs to be ensured. The auxiliary mass should exert an inertial force out of phase with respect to the displacement of the main structure. Fig. 1 (a) shows a model of a TMD in its passive from [Den Hartog 1985]. An active tuned-mass damper (ATMD) system, shown in Fig. 1 (b), is a versatile system that utilizes an additional forcing function on the mass to perform a broad range of disturbance attenuation by feedforward, feedback or both forms of control [Pare 1999]. The force that the actuator delivers to the structure is dependent upon the response of the system in which the actuator(s) is programmed and

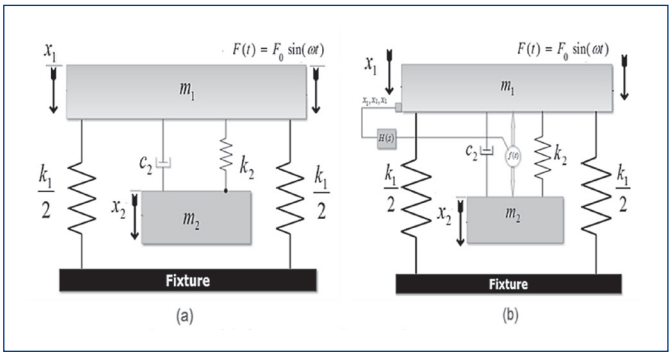

Figure 1. Model of a TMD (a) and ATMD (b) as a 2 DOF system

controlled to provide to the machine mass to hold it nearly motionless by counteracting its response. In Fig. 1 (b), it is assumed that the mass m_1 is the engine case and the mass m_2 is the absorber mass. An actuator is placed between the two masses to provide a force *f(t)*. A feedback element *H(s)* provides information about the response of the main mass m_1 and feeds it into the actuator.

3. MODELLING, SIMULATION AND VALIDATION

3.1 MECHANICAL VIBRATION MODEL FOR THE FPSE/LA

The use of simpler models as that of Fig. 2 is deemed sufficient from a dynamic point of view for this application. The subsystem (a) of Fig. 2 represents the casing of the Stirling engine which forms the primary system that contains a displacer and a piston modeled as spring-mass-damper system. Subsystem (b) represents that of the TMD. While neglecting the internal dynamics of the piston and the displacer and by assuming that the piston is causing a sinusoidal excitation in the casing, a vibration model of the Stirling engine system is proposed by approximating it as a 2-DOF system. The mass m_1 is connected by a spring of stiffness k_1 and a damping element of coefficient c_1 to ground on one end and to a passive absorber via another spring of stiffness k_2 and another damping element of coefficient c_2 on the other end. The equations of motion that describe the 2-DoF system can be represented in the form of a state-space model as follows

$$\begin{bmatrix}\dot{x}_1\\ \dot{x}_2\\ \dot{x}_3\\ \dot{x}_4\end{bmatrix} = \begin{bmatrix} 0 & 0 & 1 & 0 \\ 0 & 0 & 0 & 1 \\ \frac{-(k_1+k_2)}{m_1} & \frac{k_2}{m_1} & \frac{-(c_1+c_2)}{m_1} & \frac{c_2}{m_1} \\ \frac{k_2}{m_2} & \frac{-k_2}{m_2} & \frac{c_2}{m_2} & \frac{-c_2}{m_2} \end{bmatrix} \begin{bmatrix}x_1\\ x_2\\ x_3\\ x_4\end{bmatrix} + \begin{bmatrix}0\\ 0\\ \frac{1}{m_1}\\ 0\end{bmatrix} F(t)$$

$$\begin{bmatrix}y_1\\ y_2\\ y_3\\ y_4\end{bmatrix} = \begin{bmatrix}1 & 0 & 0 & 0\\ 0 & 1 & 0 & 0\\ 0 & 0 & 1 & 0\\ 0 & 0 & 0 & 1\end{bmatrix} \begin{bmatrix}x_1\\ x_2\\ x_3\\ x_4\end{bmatrix} \quad (1)$$

The variables x_1, x_2, x_3 and x_4 represent the primary mass and TMD's displacements and velocities respectively.

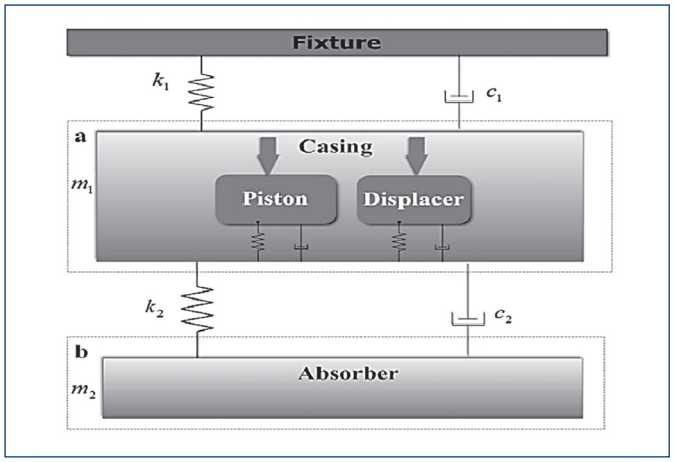

Figure 2. Dynamic model of the β-type Stirling engine showing a casing

3.2 MODEL SIMULATION

Simulation parameters
m_1 = 41,38 kg
m_2 = 8,862 kg
c_1 = 300 Ns/m
c_2 =2,7 Ns/m
k_1 =8369.4 N/m
k_2 =874640 N/m
F(t) = 1 000 sin 100 πt

Table 1. System Parameters

The Bode plot of Fig. 3 (a) shows the frequency response of the primary mass displacement. A peak occurs at 2 Hz due to the first mode of resonance of the combined system. A further peak occurs at 54.79 Hz corresponding to the second mode of vibration resonance. In fact, the first peak can be neglected since the nominal operating frequency range of the β-type Stirling engine is 50 Hz. The risk occurs towards the second peak which is very close to the operating range. Fig. 3 (b) shows the frequency response of the engine acceleration in g's between 47 Hz – 53 Hz. It reveals that the acceleration is reduced as the frequency varies to reach a minimum at 50 Hz as a result of the tuning of the TMD. The specification requires that the maximum allowed displacement of the engine case is restricted to ± 20 μm. According to the graphs, if the excitation frequency drifts from 50 Hz, the magnitudes of vibration exceed the limit and thus affect the engine operation. It can be argued that a larger damping coefficient c_2 on the TMD system is capable of broadening the bandwidth of operation of the TMD however there is a trade-off between damping and attenuation- that is – a higher damping in the TMD leads to a less attenuation on the primary mass at resonance.

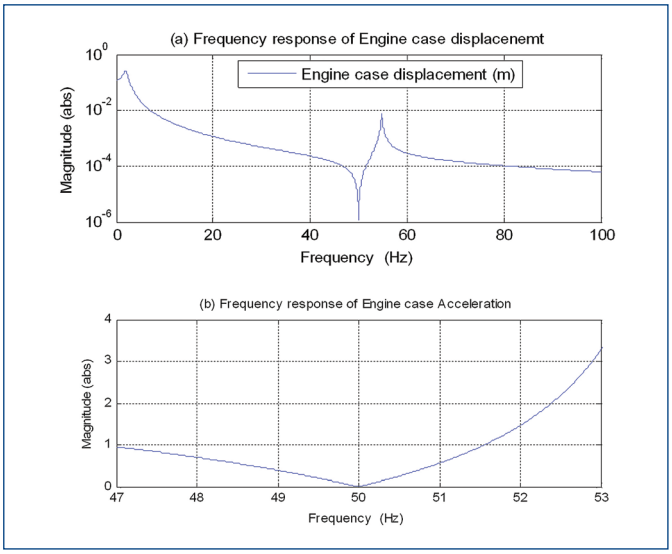

Figure 3. Frequency response of the (a) engine case displacement and (b) acceleration

3.3 MODEL VALIDATION

Fig. 4 shows the mounting of the Stirling engine and the absorber for the validation tests. The engine is fitted with an absorber that is mounted internally to the engine. In this experiment, the engine was motored by an inverter that delivers a sinusoidal excitation with varying frequency. The magnitude of the excitation force in the engine is not constant due to the varying electrical current. The magnitude of this force is estimated to be around 1 000 N based on multiplying the current through the engine with the motor constant of the engine coil. Vibration Data were collected and averaged from four MEMS accelerometers with dynamic range ± 2 g, bandwidth 1 kHz and sensitivity of 350 mv/g placed in four different locations to detect the vertical vibration. For the TMD, a separate test was carried out by vertically mounting it to an electromagnetic shaker (LDS V721). This test was performed using a sinusoidal profile between 40 Hz to 80 Hz in open loop. In fact, a closed loop control means that the shaker controller demands a constant acceleration on the shaker table throughout the sweep. However, in this case the TMD will attenuate the shaker table vibration at 50 Hz hence the open loop test. Acceleration data from the dynamic mass of the absorber and the shaker table were collected from two accelerometers of 100 mv/g sensitivity and 70 g maximum dynamic range. Fine tuning of the absorber was done by adding and removing some dynamic mass from the absorber. The theoretical transmissibility

is shown in equation 2 and the value of c_2 was validated using a reverse fitting technique of the experimental results. The results from both tests are presented in Fig 5.

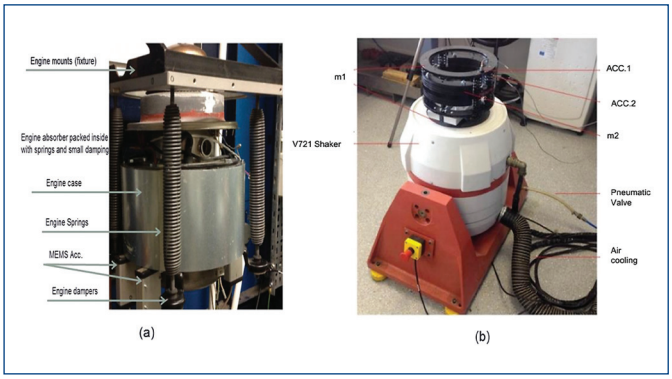

Figure 4. (a) β-type Stirling engine courtesy of Microgen Engine Corporation (MEC) and (b) Rig of the TMD

$$TR = \frac{X_{absorber}}{X_{shaker\ table}} = \frac{s^2 X_{absorber}}{s^2 X_{shaker\ table}} = \frac{c_2 s + k_2}{m_2 s^2 + c_2 s + k_2} \quad (2)$$

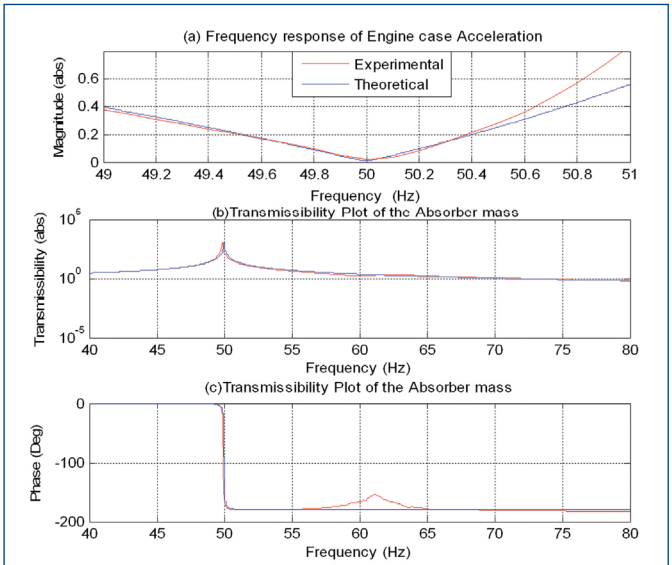

Figure 5. Theoretical Vs. Experimental data of the (a) engine case acceleration (b) Absorber Transmissibility (c) Absorber Transmissibility phase

In Fig. 5 (a), experimental data from the engine case acceleration were averaged and plotted against the theoretical results. It reveals that the acceleration is attenuated at 50 Hz due to the resonance of the TMD. After 50Hz the amplitudes of the acceleration grow larger due to the second resonance of the combined system. There appears to be a difference between both sets of data as the experimental acceleration grows larger than the theoretical one after 50 Hz. The cause of this difference is attributed to the excitation force amplitude which is assumed to be around 1 000 N in theory however in reality the magnitude of this force varies depending on frequency and loading of the engine. According to Fig. 5 (b, c), the real response of the absorber shows some dynamics around 62 Hz which didn't exist in simulation. The root cause of this discrepancy is linked to the second resonance of the combined system consisting of shaker table mass and the absorber mass which was not part of the simulated model. As a result of the obtained experimental data, the proposed model of the Stirling engine serves as a good match within the required operating range.

4. ACTIVE VIBRATION CONTROL STATEGIES FOR THE STIRLING ENGINE MODEL

The validated model of the Stirling engine is used with an additional actuating element. A generic actuator force is assumed to be situated between the two masses and is providing a generic force, *f(t)*, based on the feedback response, *H(s)*, of the system as shown previously in the Fig. 1(b).

4.1 FEEDFORWARD ZERO PLACEMENT CONTROL WITH POSITION/ACCELERATION FEEDBACK

In this type of control, the automation of the control strategy can be achieved by providing a priori knowledge of changes in excitation frequency without the need of an accurate model for the entire system. The working principle is based on re-tuning of the TMD so its frequency tracks that of the excitation one. The equations of motion (3) shown below are derived using Newton's second law.

$$\begin{aligned} m_1\ddot{x}_1 + k_1 x_1 + c_1\dot{x}_1 + k_2(x_1 - x_2) + c_2(\dot{x}_1 - \dot{x}_2) &= F(t) - f(t) \\ m_2\ddot{x}_2 + k_2(x_2 - x_1) + c_2(\dot{x}_2 - \dot{x}_1) &= f(t) \end{aligned} \quad (3)$$

It follows that the actuator force, *f(t)*, may take the following generic form

$$f(t) = -[\alpha(\ddot{x}_1 - \ddot{x}_2) + \beta(\dot{x}_1 - \dot{x}_2) + \gamma(x_1 - x_2)] \quad (4)$$

Where α, β, and γ represent the relative acceleration, velocity, and dis- placement feedback gains respectively. The closed loop transfer function can then be derived and expressed in the Laplace domain as follows

$$W(s) = \frac{X_1(s)}{F(s)} = \frac{(m_2 + \alpha)s^2 + (c_2 + \beta)s + (k_2 + \gamma)}{a_0 s^4 + a_1 s^3 + a_2 s^2 + a_3 s + a_4} \quad (5)$$

Where

$$\begin{aligned} a_0 &= m_2\alpha + m_1(m_2 + \alpha) \\ a_1 &= (m_1 + m_2)(c_2 + \beta) + c_1(m_2 + \alpha) \\ a_2 &= k_1(m_2 + \alpha) + c_1(c_2 + \beta) + (k_2 + \gamma)(m_1 + m_2) \\ a_3 &= c_1(k_2 + \gamma) + k_1(c_2 + \beta) \\ a_4 &= k_1(k_2 + \gamma) \end{aligned}$$

The transfer function *W(s)* has a zero at

$$\omega = \sqrt{\frac{k_2 + \gamma}{m_2 + \alpha}}$$

which makes it possible to cancel harmonic vibration at a given value of frequency ω by appropriate choice of relative acceleration or displacement feedback gains so that the absorber frequency matches the excitation one. If the TMD is assumed to have negligible damping then its damping coefficient is zero and therefore there is no need for a velocity feedback ($c_2 = \beta = 0$) to cancel it however when $c_2 \neq 0$, a new term is added to the numerator of *W(s)* and the velocity feedback coefficient β has to be chosen accordingly in order to zero the numerator again. It can be generalized that for the above system, a feedback force that is proportional to the relative displacement or acceleration of the two masses can alter the natural frequency of the absorber. If feedback force is proportional to relative velocity, it cannot alter the tuned frequency of the absorber but only the quality factor. The formulae that relate the required gain γ and α to produce a frequency shift to the absorber frequency so it tracks the excitation one are shown below

$$\gamma = m_2(\omega^2 - {\omega_0}^2) \quad (6)$$

$$\alpha = m_2\left(\frac{{\omega_0}^2}{\omega^2} - 1\right) \quad (7)$$

where ω_0 is the original natural frequency of the TMD and ω the excitation frequency.

The following graph shows the required gains γ and α against frequency increment for the Stirling engine under study.

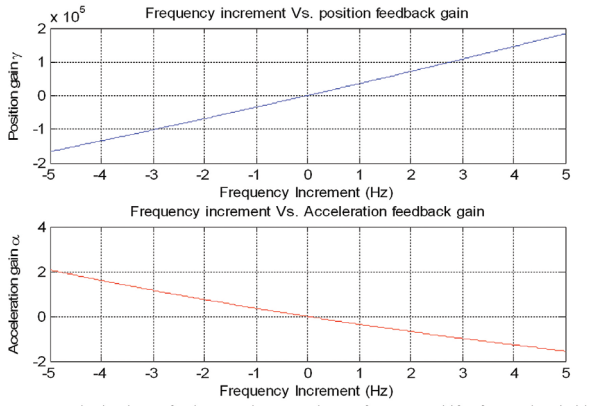

Figure 6. Required values of gains γ and α to produce a frequency shift of 10 Hz bandwidth

4.2 LINEAR QUADRATIC CONTROL (LQ) WITH FULL STATE FEEDBACK

Optimal control is one of the modern control methods that are commonly used in the area of vibration reduction. The optimal control method achieves the optimal solution by calculating the feedback gains that result from the minimization of a cost function or a performance index based on previous knowledge of the system [Preumont 2011]. In other words, the feedback gains are optimized in order to achieve a control *u(t)* that minimizes a cost function expressed as

$$J = \int_0^\infty (x^T Q x + u^T R u) dt \tag{8}$$

For the purpose of deriving the LQ control dynamics, the state space model can be defined as in equation 1. The matrices Q and R represent the states and input variables respectively and their coefficient are chosen following a heuristic procedure based on the expected magnitudes of the system states. The steady state solution of the optimal problem that determines the required actuator force becomes

$$f(t) = -[K]x \tag{9}$$

The vector x is a full state-feedback vector with all the states and *K* is a constant gain matrix obtained by solving a non-linear Algebraic Riccati equation (ARE). Two major drawbacks arise with the LQ control strategy. First of all, good knowledge of the model dynamics is required to obtain the gain matrices, inaccurate modelling may result in the poor control performance. Secondly, the LQ control requires access to the full state variables which is not always possible to access due to many factors such as the physical limitations in the sense of the number of sensors that can be used in addition to the processing power that increases with the increase of data measurement. Practically speaking it is either not feasible or prohibitively expensive to measure all the states, thus feedback control design often requires state variable estimation. An observer is a dynamic system with control inputs and measured responses, and an output that estimates the state vector. It is based on designing a system similar to the original system – that is using the same eigenvalues as the original system as well as adding feedback correcting element with a gain *L* so it estimates the states of the real system. Fig. 7 presents the working principle of a state observer based on state space representation.

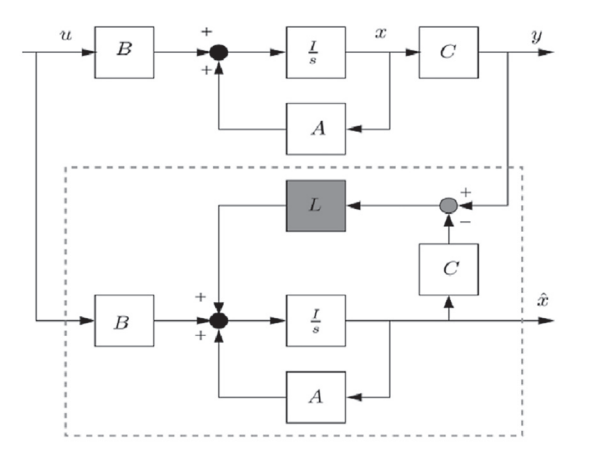

Figure 7. Closed loop state observer design

5. ACTIVE VIBRATION CONTROL SIMULATION: FREQUENCY DOMAIN

Simulation parameters

$$Q = \begin{bmatrix} 5e8 & 0 & 0 & 0 \\ 0 & 0 & 0 & 0 \\ 0 & 0 & 1e7 & 0 \\ 0 & 0 & 0 & 0 \end{bmatrix} \quad R = \begin{bmatrix} 5e-5 & 0 \\ 0 & 15e-6 \end{bmatrix}$$

$$K = \begin{bmatrix} 2e6 & 8e5 & 4e5 & 1500 \\ -0.8e6 & -0.2e6 & -0.13e6 & 1400 \end{bmatrix}$$

$$L = \begin{bmatrix} 0.5e-12 & -0.5e-12 & 0.05e-12 & -0.005e-12 \\ 0 & 0 & 0 & 0 \\ 0 & 0 & 0 & 0 \\ 0 & 0 & 0 & 0 \end{bmatrix}$$

Table 2: LQ with state observer control parameters

This section shows the simulation results of the proposed control strategies in the frequency domain with the excitation frequency varied from 45 Hz to 55 Hz. The parameters of Tab. 1 are used. The graphs of Fig. 8 show the frequency response of the engine case displacement with feedforward control on. Originally, the TMD in the Stirling engine is tuned at 50 Hz. As the excitation frequency is varied, the feedforward control with zero placement strategy with either position or acceleration feedback gains automatically determines a gain online that alters the TMD's natural frequency to track the excitation frequency. The excitation has a magnitude of 1 000 N and frequency that varies from 45 Hz to 55 Hz in 1 Hz step. This control technique doesn't only attenuate the vibration of the system at a particular frequency, but it also shifts the resonant frequency of the entire system. That is, the vibration can be attenuated even when the excitation hit the resonance of the original system.

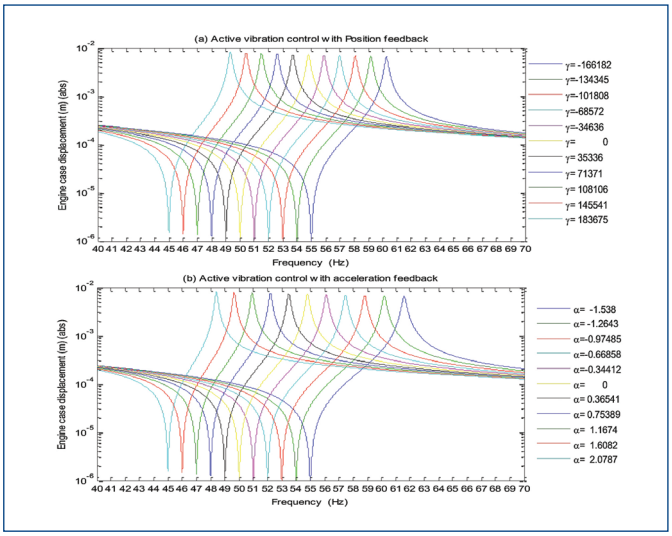

Figure 8. Frequency response of the engine case displacement with feedforward zero-placement control (a) position feedback (γ)

For LQ control, the Bode diagram in Fig. 9 shows the response of the engine case displacement as per the effect of LQ control. The parameters of Tab. 1, 2 are used for carrying out the simulations with LQ control. It is shown that the control behavior of the LQ is different to that of the previous control technique. The LQ control relies on one gain K that is optimized to operate over a wide range of frequencies as presented below. By comparing the two control strategies from the frequency domain, it appears that the zero placement technique achieves better attenuation than the LQ control. In fact, for the zero placement control, the full model dynamics do not necessarily have to be available unlike with LQ control. Furthermore, zero placement is achieved much easier than that of the LQ control because it doesn't require the solution of an ARE.

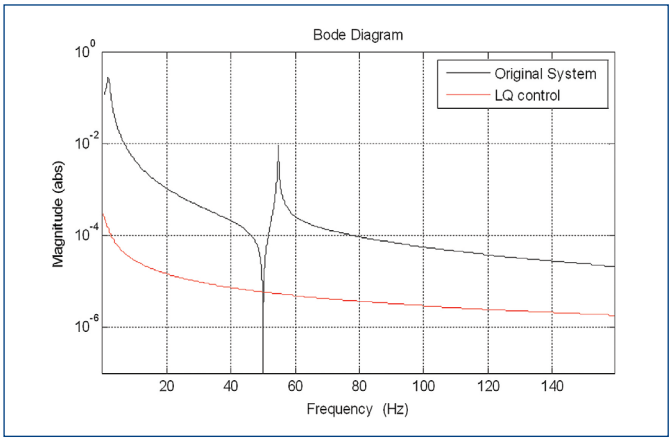

Figure 9. Frequency response of the engine case displacement with the effect of LQ control

6. ELECTROMECHANCIAL MODELLING AND SIMULATION WITH LINEAR VOICE COIL MOTOR (VCM)

A VCM actuator is added to the original system. The equations that relate the dynamic mechanical system to the electrical system with the VCM are presented below

$$\begin{cases} m_1\ddot{x}_1 + k_1x_1 + c_1\dot{x}_1 + k_2(x_1 - x_2) + c_2(\dot{x}_1 - \dot{x}_2) = F - f_{act} \\ m_2\ddot{x}_2 + k_2(x_2 - x_1) + c_2(\dot{x}_2 - \dot{x}_1) = f_{act} \\ V_{act} = Ri_{act} + L\dfrac{di_{act}}{dt} + k_m(\dot{x}_2 - \dot{x}_1) \\ V_{act} = PID(i_{ref} - i_{act}) \\ f_{act} = k_m i_{act} \\ e = i_{ref} - i_{act} \\ PID = k_p e + k_i \int edt + k_d \dfrac{d}{dt}(e) \end{cases} \qquad \begin{cases} x_1 = x_1 \\ x_2 = x_2 \\ x_3 = q_{act} \\ x_4 = \dot{x}_1 \\ x_5 = \dot{x}_2 \\ x_6 = \dot{x}_3 = \dot{q}_{act} \end{cases} \tag{10}$$

x_1 : *Engine case displacement*
$\dot{x}_1$: *Engine case velocity*
x_2 : *Absorber mass displacement*
$\dot{x}_2$: *Absorber mass velocity*
q_{act}: *actual VCM charge*
$\dot{q}_{act}$: *actual VCM current*
q_{ref} : *desired VCM charge*
$\dot{q}_{ref}$: *desired VCM current*
R: *motor coil resistance*
L: *motor coil inductance*
k_m: *motor constant*

The VCM is modelled as an *RL* circuit with V_{act} and i_{act} representing the voltage across and the current through the VCM terminals. The terms *R, L* and k_m represent the motor coil inductance, resistance, and the motor constant respectively. The mass m_1 is the engine case mass added to the VCM stationary base and the absorber stationary mass. The mass m_2 includes the dynamic mass of the absorber and the VCM's moving coil. Here it is assumed that the back electromotive force constant is the same as k_m. The constants k_p, k_i and k_d represent the PID controller's gains. The term i_{ref} refers to the reference current that is inversely proportional by k_m to the control force generated by the active damping control strategy. The inputs to the PID controller are the VCM reference current i_{ref} and the actual current i_{act}. The control force f_{atc}, generated by either control strategy, is proportional to the VCM motor current by a factor k_m. The resulting state space representation of the coupled electromechanical system is developed and shown below alongside the simulation parameters.

$$\begin{bmatrix} \dot{x}_1 \\ \dot{x}_2 \\ \dot{x}_3 \\ \dot{x}_4 \\ \dot{x}_5 \\ \dot{x}_6 \end{bmatrix} = \begin{bmatrix} 0 & 0 & 0 & 1 & 0 & 0 \\ 0 & 0 & 0 & 0 & 1 & 0 \\ 0 & 0 & 0 & 0 & 0 & 1 \\ \dfrac{-(k_1+k_2)}{m_1} & \dfrac{k_2}{m_1} & 0 & \dfrac{-(c_1+c_2)}{m_1} & \dfrac{c_2}{m_1} & \dfrac{-k_m}{m_1} \\ \dfrac{k_2}{m_2} & \dfrac{-k_2}{m_2} & 0 & \dfrac{c_2}{m_2} & \dfrac{-c_2}{m_2} & \dfrac{k_m}{m_2} \\ 0 & 0 & \dfrac{-k_i}{L+k_d} & \dfrac{-k_m}{L+k_d} & \dfrac{k_m}{L+k_d} & \dfrac{-R-k_p}{L+k_d} \end{bmatrix} \begin{bmatrix} x_1 \\ x_2 \\ x_3 \\ x_4 \\ x_5 \\ x_6 \end{bmatrix} + \begin{bmatrix} 0 & 0 & 0 & 0 \\ 0 & 0 & 0 & 0 \\ 0 & 0 & 0 & 0 \\ \dfrac{1}{m_1} & 0 & 0 & 0 \\ 0 & 0 & 0 & 0 \\ 0 & \dfrac{k_i}{(L+k_d)} & \dfrac{k_p}{L+k_d} & \dfrac{k_d}{(L+k_d)} \end{bmatrix} \begin{bmatrix} F \\ q_{ref} \\ \dot{q}_{ref} \\ \ddot{q}_{ref} \end{bmatrix}$$

$$y = \begin{bmatrix} 1 & \cdots & 0 \\ \vdots & \ddots & \vdots \\ 0 & \cdots & 1 \end{bmatrix} \begin{bmatrix} x_1 \\ x_2 \\ x_3 \\ x_4 \\ x_5 \\ x_6 \end{bmatrix} + \begin{bmatrix} 0 & 0 & 0 & 0 \\ 0 & 0 & 0 & 0 \\ 0 & 0 & 0 & 0 \\ 0 & 0 & 0 & 0 \\ 0 & 0 & 0 & 0 \\ 0 & 0 & 0 & 0 \end{bmatrix} \begin{bmatrix} F \\ q_{ref} \\ \dot{q}_{ref} \\ \ddot{q}_{ref} \end{bmatrix} \tag{11}$$

Mechanical	Electrical
$m_1 = 41.38 + m_{VCM} kg$	$L = 2.1\ mH$
$m_2 = 8.862 + m_{coil} kg$	$R = 3\ \Omega$
$c_1 = 300\ Ns/m$	$Km = 22.2\ N/A$
$c_2 = 2.7\ Ns/m$	$m_{VCM} = 4.15\ kg$
$k_1 = 9122.8\ N/m$	$m_{coil} = 0.621\ kg$
$k_2 = 935930\ N/m$	
$F(t) = 1000 \sin(100\pi t)\ N$	

$$Q = \begin{bmatrix} 1e7 & 0 & 0 & 0 & 0 & 0 \\ 0 & 0 & 0 & 0 & 0 & 0 \\ 0 & 0 & 0 & 0 & 0 & 0 \\ 0 & 0 & 0 & 3e5 & 0 & 0 \\ 0 & 0 & 0 & 0 & 0 & 0 \\ 0 & 0 & 0 & 0 & 0 & 0 \end{bmatrix} \quad R = \begin{bmatrix} 1e-6 & 0 & 0 & 0 \\ 0 & 2e-9 & 0 & 0 \\ 0 & 0 & 1e-5 & 0 \\ 0 & 0 & 0 & 1e-10 \end{bmatrix}$$

$$K = \begin{bmatrix} 2.3e6 & 8.7e5 & 0.11 & 5e5 & 871 & -2.7 \\ -8e6 & -1.6e6 & -0.17 & -1.6e6 & 0.03e6 & 10.2 \\ -0.2e6 & -0.04e6 & -0.0042 & -0.03e6 & 745 & 0.25 \\ 0 & 0 & 0 & 0 & 0 & 0 \end{bmatrix}$$

$$L^T = \begin{bmatrix} 20e-12 & 0 & 0 & 0 & 0 \\ 10e-8 & 0 & 0 & 0 & 0 \\ 0.663 & 0 & 0 & 0 & 0 \\ 6e-6 & 0 & 0 & 0 & 0 \\ -3.3e-6 & 0 & 0 & 0 & 0 \\ 0.1 & 0 & 0 & 0 & 0 \end{bmatrix}$$

$kp = 150 \quad ki = 1 \quad kd = 0$

Table 3. Electromechanical system parameters

The simulation was performed for a total time of 60 seconds with the excitation frequency being incremented automatically by 1 Hz every 5 seconds of simulation time from 45 Hz to 55 Hz. The actuator force f_{act} is determined by either feedforward or LQ control strategies accordingly. In the case of LQ control, the matrix gain is obtained similar to that of the original system (i. e. penalizing the same states) using the Bryson's rule (Tab. 3). Only the third row of K is considered since the interest is in the reference current q_{ref} only.

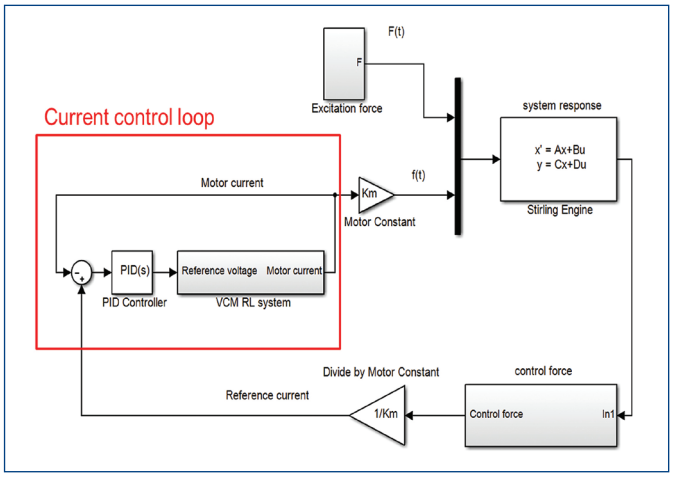

Figure 10. Control system representation

The graphs of Fig. 11 shows the cases of no control, feedforward control, and LQ with state observer control for the engine displacement and required actuator strokes. In addition to that, the estimated VCM voltage and current requirements are shown.

The simulation results show that both the LQ and feedforward control strategies can successfully attenuate the vibration of the Stirling engine case to the required specification of 20 μm over a bandwidth of 47 Hz –

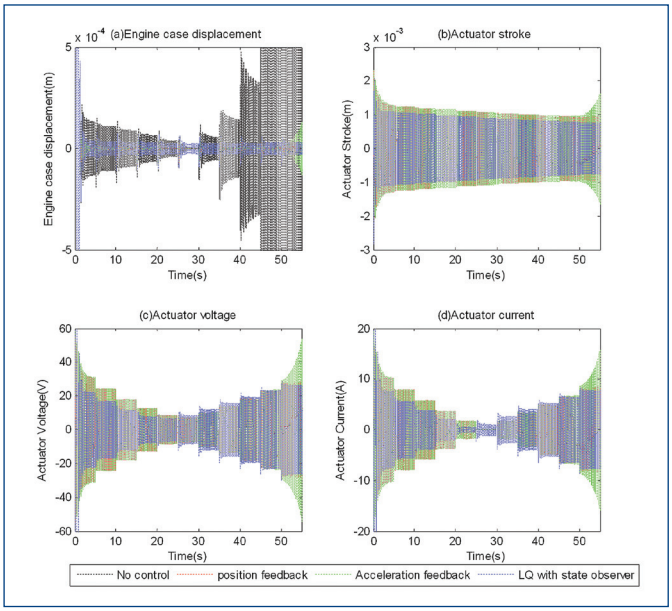

Figure 11. Time domain simulation results with two control strategies

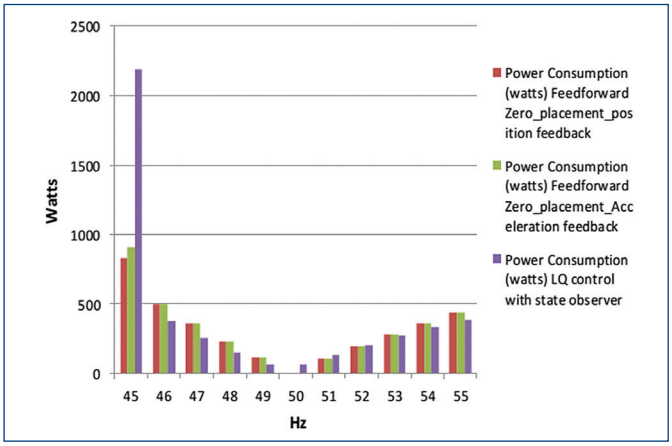

Figure 12. VCM estimated power consumption

53 Hz. Moreover, the values of actuator strokes, current, and voltage are almost identical irrespective of which control strategy is employed. To discuss the results in more detail, according to the graphs of Fig. 11, it is revealed that as the excitation frequency shifts on either side from 50 Hz, the engine case displacement grows larger exceeding the maximum allowed amplitude in the case when control is off. In fact, as the excitation frequency shifts rightwards from 50 Hz, the amplitudes grow much larger than the case of shifting leftwards. The larger amplitudes for frequencies above 50 Hz are expected as the natural frequency of the combined system is located at approximately 54.8 Hz. When control is on, the graph of Fig. 11 (a) shows that as the excitation frequency deviates from 50 Hz, the displacement of the engine case is still attenuated to almost the same magnitudes as at 50 Hz indicating that the VCM is capable of re-tuning the absorber frequency. Similarly, in the case of LQ control, the VCM succeeds to provide the necessary force that would minimize the displacement of the engine case. This is also the case in Fig. 11 (d) where the current of the VCM increases when the excitation frequency furthers away from 50 Hz. The bar chart of Fig. 12 shows the estimated power consumption of the VCM. It can be seen that for the LQ control case, a large power requirement at 45 Hz is required. Actually, this is due to the high transients occurring in the case of the LQ control. A further tuning of the LQ gain matrices can possibly avoid this transient. In reality, the grid frequency never fluctuates from 50 Hz to 45 Hz immediately.

7. TIME DELAY: EFFECT ON CONTROL STABILITY

The general form of the actuator force is written as shown in equation 4. If a time delay is assumed to exist in the control action, the general force of the control force can be re-written as follows

$$f_{act}(t-\tau) = d(t-\tau)[\alpha(\ddot{x_1} - \ddot{x_2}) + \beta(\dot{x_1} - \dot{x_2}) + \gamma(x_1 - x_2)] \quad (12)$$

The Laplace transform of this delay of $d(t-\tau)$ can be expressed by $e^{-\tau s}$. It is not possible to study the poles of the transfer function while the delay is represented exponentially. Hence, the most obvious polynomial expansion of the exponential is the Taylor series. The first order of Taylor approximation assuming a sinusoidal force of period T in the frequency domain becomes

$$\begin{cases} e^{-\tau s} \xrightarrow{s=j\omega} e^{-j\tau\omega} = e^{-j\tau\frac{2\pi}{T}} = e^{-j2\pi\tau_n} \\ e^{-\tau s} \approx 1 - \tau s \xrightarrow{yields} e^{-j2\pi\tau_n} \approx 1 + j2\pi\tau_n \end{cases} \quad (13)$$

Where τ_n is the normalised delay, the relative error is defined as

$$e_r = \left| \frac{e^{-j2\pi\tau_n} - (1 + j2\pi\tau_n)}{e^{-j2\pi\tau_n}} \right| \cdot 100[\%] \quad (14)$$

Assuming that the excitation is sinusoidal, Fig. 13 shows the percentage of error in the Taylor approximation as a function of the normalized delay. It was found that in order for the Taylor approximation to be 10 % less, the delay has to be 10 times less than the operating period T with the first order approximation whereas it has to be 6.6 times less with second order approximation in order for the Taylor estimation to be accurately representative. For the purpose of the application in this research, the first Taylor approximation is assumed to be good enough. The transfer function of the entire system is obtained by modal reduction where the electromechanical equations were substituted into the equations of motion. Hence a SISO system with the excitation force as the only input was obtained.

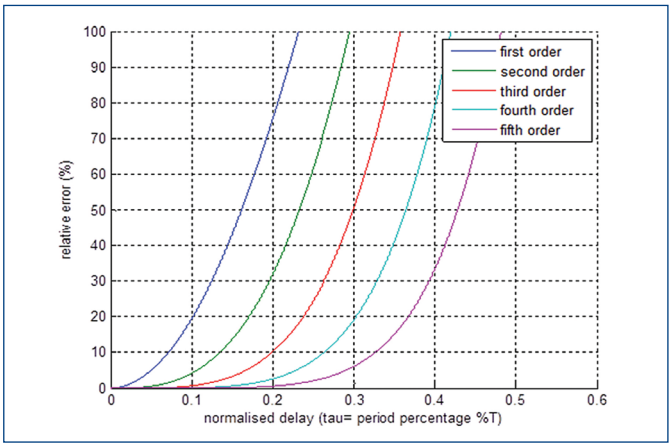

Figure 13. Percentage error between the original delay function and its Taylor series expansion approximation

7.1 FEEDFORWARD CONTROL

The following set of graphs show the system poles as a function of time delay for the feedforward control with position and acceleration feedback at for ten different excitation frequencies covering the operating range. According to Fig. 14 (a), when the excitation frequency is less than 50 Hz delays do not destabilize the system and in the case of excitation above 50 Hz, the system is only stable before a certain amount of time delay around 0.2 ms at 51 Hz due to one of the poles changing to positive. The amount of acceptable time delay reduces as the frequency increases.

The effect of time delay on the control with acceleration feedback is shown in Fig 14 (b). Unlike the pervious case, it appears that the time delay not only has an effect on stability before but also after the 50 Hz due to the first pole changing to positive. Actually, the amount of

acceptable time delay decreases as the frequency moves from 50 Hz. One common aspect between the two feedforward zero-placement cases is that the amount of acceptable time delay after 50 Hz is quite similar.

also that a zero derivative gain of the PID controller must be chosen otherwise the system will be unstable. The following plot shows the effect of time delay on the system poles with LQ control. According to Fig. 15, a delay if around 0.4 ms could deteriorate the control action

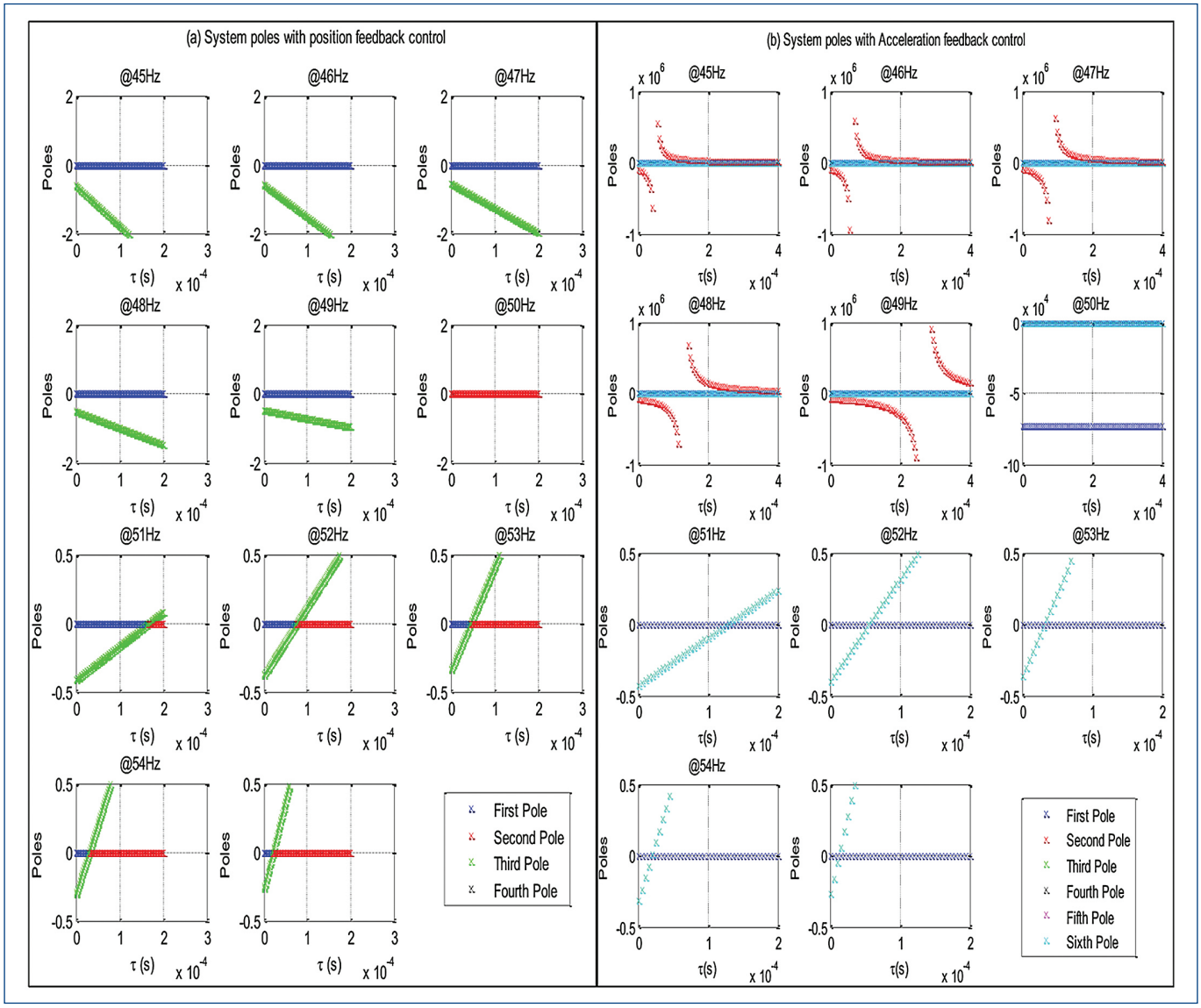

Figure 14. System poles real values as a function of time delay with position feedback

7.2 LQ CONTROL

In the case of LQ control, since only one gain matrix is available, the study of delay is done once for that particular gain. It has to be noted and lead to instability. Hence, at the implementation stage, careful consideration has to be given to the hardware and control code in order to guarantee safe control.

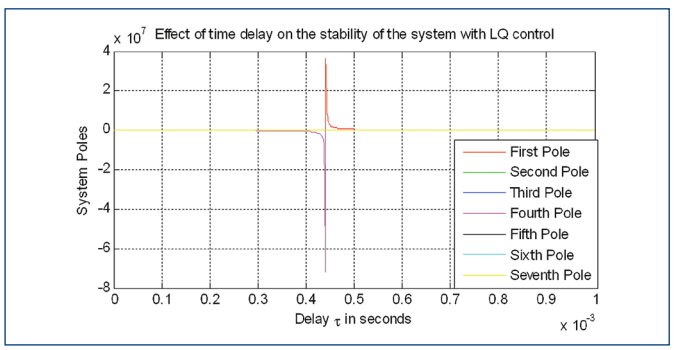

Figure 15. System poles real values as a function of time delay with position feedback

8. ACTIVE VIBRATION CONTROL: COMPARISON

	Feedforward	LQ
Active Damping	Both control techniques succeed in attenuating the vibration of the engine from a theoretical point of view. VCM stroke, force, voltage, current, and power are very similar in both cases	
Model Dynamics	Requires knowledge of the frequency. No accurate model required	Requires accurate modelling and a state observer
Operation	Tracks excitation frequency to alter that of the ATMD	It provides a single gain that works over a wider bandwidth
Gain Tuning	Online calculation of the gains is required however it is fairly straight forward	Gain is calculated offline however it is more difficult to obtain the optimal gains
Time Delay	Could be destabilized after a certain time delay depending on excitation frequency	Could be destabilized but allows for more time delay irrespective of excitation frequency

Table 4. Comparison of the control strategies

9. CONCLUSION

New grid connection/disconnection regulations for small scale generators have imposed challenging design constraints in FPSE/LA generators when the machine is grid connected. Currently, this type of machine is cost effective when it operates in a narrow bandwidth of frequencies. The use of active control strategies has proven to be a potential solution to meet new regulations. As a result, this work investigated the conversion of the passive TMD that already exists in the β-type Stirling engine into an ATMD. A simplified model of the real structure was developed, simulated and later validated using real parameters of the β-type Stirling engine. Feedforward zero-placement and optimal LQ control strategies have been investigated from a frequency and time domain perspectives. The results showed that both strategies have succeeded to minimize the vibration of the Stirling engine case to limit the peak amplitude within the value of 20 μm over a wider bandwidth. An electromechanical model was further developed including a linear VCM. The simulation of the electromechanical model showed that the VCM succeeds to mitigate the vibration of the Stirling engine and parameters such as voltage, current, power consumption were obtained for the required forces and strokes. Finally, a study of the effect of delays on the stability of electromechanical system has been carried out. It was found that delays affect the stability of the control depending on the control strategy followed the frequency of operation. The results presented in this study could also be generalized for any 2-DOF system and not only for the application of this research.

ACKNOWLEDGMENT

We are very grateful to Microgen Engine Corporation (MEC) for providing the necessary engineering data required for modelling, simulation, and testing carried out in this work.

REFERENCES

[Chang 1995] Chang, C. and Yang, H. T. Control of buildings using active tuned mass dampers. Journal of Engineering Mechanics, 121(3), pp. 355-366 (1995)

[Den Hartog 1985] Den Hartog, J. P. Mechanical Vibrations.Dover Publications. (1985)

[Harrison 2004] Harrison, J. Micro Combined Heat & Power (CHP) for housing, 3rd International Conference on Sustainable Energy Technologies, Nottingham, UK 2004 (2004)

[Hassan 2014] Hassan, A., Torres-Perez, A., Kaczmarczyk, S. and Picton, P. Active vibration control strategies for a Free Piston Stirling Engine generator, Mechatronika (ME), 2014 16th International Conference on Mechatronics, 2014, pp. 381-387 (2014)

[Johnson 2012] Johnson, W., Long, R., Nelson, M. and Mascarenas, D. Embedded Active Vibration Cancellation of a Piston-Driven Cryocooler for Nuclear Spectroscopy Applications. Springer New York, pp. 377-384 (2012)

[Kwak 2007] Kwak, M. K. and Heo, S. Active vibration control of smart grid structure by multiinput and multioutput positive position feedback controller. Journal of Sound and Vibration, 304(1), pp. 230-245 (2007)

[Li 2003] Li, C., Liu, Y. and Wang, Z. Active multiple tuned mass dampers: a new control strategy. Journal of Structural Engineering, 129(7), pp. 972-977 (2003)

[Liu 2013] Liu, Y. and Wu, W. Active Vibration Isolation Using a Voice Coil Actuator with Absolute Velocity Feedback Control. International Journal of Automation and Smart Technology, 3 (4), pp. 221-226 (2013)

[Mead 1999] Mead, D. J. Passive vibration control. Wiley (1999)

[Nagashima 2001] Nagashima, I. Optimal displacement feedback control law for active tuned mass damper. Earthquake Engineering & Structural Dynamics, 30(8), pp. 1221-1242 (2001)

[Pare 1999] Pare, T. E. Hybrid H2 CONTROL Design for Vibration Isolation. Journal of Sound Vibration, 226, pp. 25-39 (1999)

[Park 2008] Park, K., Choi, D., Ozer, A., Kim, S., Lee, Y. and Joo, D. A voice coil actuator driven active vibration isolation system with the consideration of flexible modes. Review of Scientific Instruments, 79(6), pp. 065106 (2008)

[Preumont 2011] Preumont, A. Vibration control of active structures: an introduction. Springer (2011)

[Rao 1990] Rao, S. S. Mechanical vibrations. Addison-Wesley (1990)

[Ross Jr. 2003] Ross Jr., R. G. Vibration suppression of advanced space cryocoolers- An overview. Smart Structures and Materials 2003, 5052, pp. 1-12 (2003)

[Walker 1980] Walker, G. Stirling engines. Clarendon Press (1980)

[Yan 1999] Jan, N., Wang, C. and Balendra, T. Optimal damper characteristics of ATMD for buildings under wind loads. Journal of Structural Engineering, 125(12), pp. 1376-1383.(1999)

CONTACTS

Ali Hassan
The University of Northampton
School of Science and Technology, St. George's Avenue
Avenue campus, NN2 6JD, Northampton
United Kingdom
tel.:+44 1 604 893 632

e-mail:
ali.hassan@northampton.ac.uk, ali.ab.hassan@gmail.com
Angel.TorresPerez@northampton.ac.uk
Stefan.kaczmarczyk@northampton.ac.uk
Phil.picton@northampton.ac